https://doi.org/10.5194/egusphere-2025-573
Preprint. Discussion started: 19 March 2025

Ocean-Induced Weakening of George VI Ice Shelf

Ann-Sofie P. Zinck[1], Bert Wouters[1], Franka Jesse[2], and Stef Lhermitte[3,1]

[1]Delft University of Technology, Delft, The Netherlands
[2]Utrecht University, Utrecht, The Netherlands
[3]KU Leuven, Leuven, Belgium

Correspondence: Ann-Sofie P. Zinck (a.p.zinck@tudelft.nl)

Abstract. Channelized basal melting is a critical process influencing ice shelf weakening, as basal channels create zones of thinning and vulnerability that can potentially lead to ice shelf destabilization. In this study, we reveal and examine the rapid development of a channel within the George VI Ice Shelf's extensive channelized network, characterized by a 23 m surface lowering over a nine-year period. We study changes in ice flow, ocean circulation and heat potential as possible drivers behind the channel, under the hypotheses that it is either a fracture, a basal melt channel, or a combination of the two. Our findings show that the onset of this channel coincides with significant changes in ocean forcing, including increased ocean temperatures and salinity, that occurred during the 2015 El Niño Southern Oscillation event. Modelling of basal melting further suggests that channel re-routing has taken place over this nine-year period, with the channel serving as a basal melt channel in the latest years. We further observe subtle shifts in ice flow indicative of fracturing. Our findings thus indicate that this channel likely contributes to the weakening of an already thin ice shelf through a combination of basal melting and fracturing. These findings offer insight into how similar potentially destabilizing processes could unfold on other Antarctic ice shelves. Monitoring the evolution of this channel and its impact on ice shelf integrity will be critical for understanding the mechanisms of ice shelf retreat, especially on heavily channelized ice shelves.

1 Introduction

The future evolution of the Antarctic Ice Sheet and its potential sea level contribution in a changing climate is highly uncertain (IPCC, 2023), largely due to the unknown response of ice shelves (Pattyn and Morlighem, 2020; Bamber et al., 2022; van de Wal et al., 2022). Ice shelves play a critical role in buttressing the ice sheet (Fürst et al., 2016) and their weakening or eventual collapse can accelerate ice flow across the grounding line, which in turn contributes to sea level rise (Pattyn and Morlighem, 2020; van de Wal et al., 2022). It is therefore crucial to understand the processes that lead to ice shelf weakening to better constrain uncertainties in sea level rise projections.

Basal melting is one such process known to weaken ice shelves (Pritchard et al., 2012; Silvano et al., 2016) and has been linked to the collapse of Wordie Ice Shelf (Doemgaard et al., 2024). Basal melting is often driven by the intrusion of Circumpolar Deep Water (CDW), a relatively warm water mass located at depth beyond the continental shelf (Silvano et al., 2016). In some regions of Antarctica, the continental shelf's bathymetry allows CDW to flow over it, enabling this warm water to reach ice shelf cavities (referred to as warm cavity ice shelves). This phenomenon occurs particularly in the Amundsen and

https://doi.org/10.5194/egusphere-2025-573
Preprint. Discussion started: 19 March 2025

Bellingshausen Seas - where the Wordie Ice Shelf was located - which experience some of the highest basal melt rates on the continent (Rignot et al., 2013; Davison et al., 2023). Although basal melting is most pronounced near the grounding zone due to the pressure-dependent freezing point of seawater (Silvano et al., 2016), the resulting meltwater plume usually travels from the grounding zone towards the ice shelf front, thereby carving basal channels in the ice (Alley et al., 2022). These channels, which are more prominent in warm cavity ice shelves (Alley et al., 2016), represent potential zones of weakness due to their reduced thickness and elevated melt rates relative to their surroundings (Alley et al., 2022).

Basal channels are dynamic features that do not necessarily remain in a steady state. They can experience changes in melt intensity, fracturing, and re-routing. In warm cavity ice shelves, the magnitude of melting within channels and across the entire ice shelf is primarily influenced by the volume and temperature of CDW entering the ice shelf cavity (Dutrieux et al., 2014). These oceanic conditions can, in turn, be affected by larger climatic phenomena such as the El Niño Southern Oscillation (ENSO, Huguenin et al., 2024). Increased availability or higher temperatures of CDW can thus lead to enhanced thinning through basal melting (Paolo et al., 2018).

Basal channels can also be associated with transverse fracturing, a phenomenon observed on several ice shelves, including Pine Island, Nansen, Moscow University, and Totten (Dow et al., 2018; Alley et al., 2024). These fractures, driven by extensional stresses within the ice (Dow et al., 2018), have triggered major calving events on Nansen and Pine Island ice shelves (Dow et al., 2018; Alley et al., 2024, 2022). Although extensional stresses are considered a primary driver, variations in meltwater availability within channels may also contribute to fracture formation (Alley et al., 2022). In addition to transverse fracturing, longitudinal fractures within basal channels have been documented (Vaughan et al., 2012; Dutrieux et al., 2013), potentially leading to full-thickness fractures and eventual ice shelf retreat (Alley et al., 2022).

The interactions between basal channels, fractures, and CDW-variations are highly complex, reflecting significant knowledge gaps in channel dynamics. Beyond changes in melt magnitude and fracturing, basal channels have been observed to migrate laterally or re-route entirely. Examples of such behavior include channels on the Getz (Chartrand and Howat, 2020) and Roi Baudouin (Drews et al., 2020) ice shelves, as well as other ice shelves in the Amundsen and Bellingshausen Sea sectors (Alley et al., 2024). Lateral channel migration, often in the direction favored by the Coriolis effect, has been linked to increased ocean heat availability (Alley et al., 2024). Similarly, the re-routing of a meltwater plume on Thwaites Ice Shelf has been observed to follow pre-existing fractures, underscoring the interplay between channel dynamics and ice shelf structure (Alley et al., 2024).

The importance of high-resolution basal channel melt rates on ice shelf weakening was emphasized using Basal melt rates Using REMA and Google Earth Engine (BURGEE, Zinck et al., 2024a). The high-resolution BURGEE melt data reveal a peculiar, and to our best knowledge so far unreported, channel on George VI Ice Shelf with high melt rates near extensive channelization (Fig. 1). The channel appears to intersect and alter other channels in the area, suggesting significant changes in the channel system during the BURGEE period (2010–2022). Given the channel's location in a heavily channelized area and its proximity to the southern ice shelf front which has been persistently retreating since 1947 (Smith et al., 2007), this channel poses a potential risk of further retreat.

In this study, we examine the potential drivers behind the formation and evolution of this newly observed channel on the George VI Ice Shelf (Fig. 1). Using high-resolution surface elevation and basal melt rate data, we assess temporal changes in

https://doi.org/10.5194/egusphere-2025-573
Preprint. Discussion started: 19 March 2025

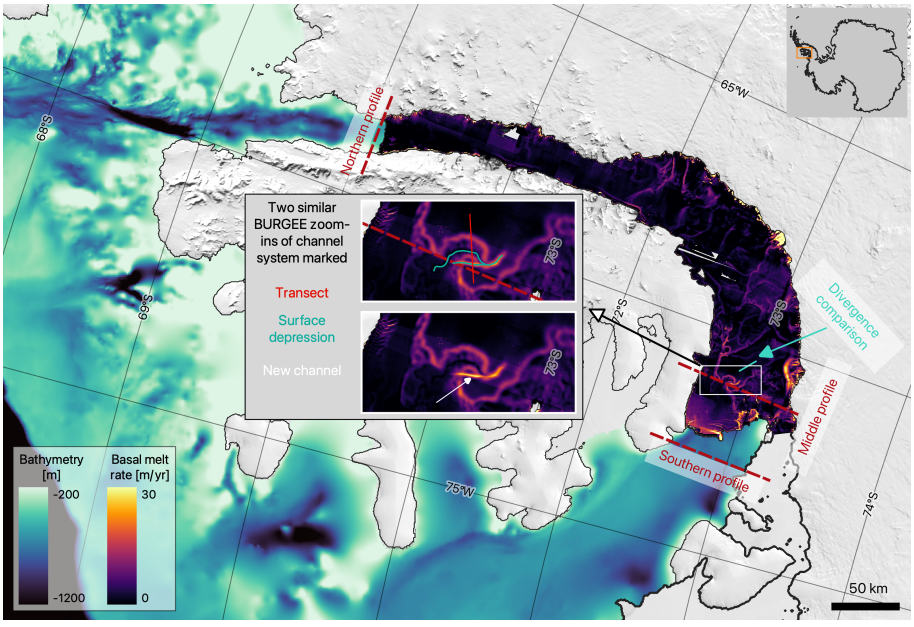

Figure 1. A map of the study area (George VI Ice Shelf) with BURGEE basal melt rates and bathymetry from BedMachineV3 (Morlighem et al., 2020; Morlighem, 2022). The grounding line and ice shelf extent are from BedMachineV3 (Morlighem et al., 2020; Morlighem, 2022). The three profiles marked (Southern, Middle, and Northern) refer to the profiles in Fig. 6. The transect marked as "Divergence comparison" refers to the transect used for assessing the root-mean-square error of the divergence in Fig. 5. Two similar zoom-ins of the highly channelized area marked by the white square shows BURGEE melt rates both with the approximate location of the surface depression of the old and new channel in year 2016 in teal, the new channel pointed out by the white arrow, as well as the red transect used in Fig. 4 and 5.

channel morphology. Furthermore, we explore the roles of ice flow dynamics, ocean circulation, and ocean forcing as potential contributors to channel evolution. Finally, we employ a basal melt model with realistic ocean forcing and ice shelf geometries from two time periods to investigate the possibility of channel re-routing within the observed network. This multi-faceted approach aims to advance our understanding of the processes driving rapid channel formation.

2 Study area

Our study area focuses on the region surrounding the newly identified channel on the George VI Ice Shelf located near the southern ice shelf front, as well as the two entrances to its ice shelf cavity where CDW flows in (Fig. 1). The analysis spans the BURGEE period from 2010 to 2022.

George VI Ice Shelf is particularly vulnerable due to its already thin state and ongoing thinning (Smith et al., 2007; Davison et al., 2023). The ice shelf experiences significant melting both from its surface (de Roda Husman et al., 2024; van Wessem et al., 2023) and its base (Davison et al., 2023), making it susceptible to structural weakening. Adding to this vulnerability, studies have shown that parts of the firn layer of the ice shelf are saturated to levels that could facilitate hydrofracturing, while

https://doi.org/10.5194/egusphere-2025-573
Preprint. Discussion started: 19 March 2025

other areas are approaching similar thresholds with only minor increases in temperature (van Wessem et al., 2023). This dual weakening mechanism highlights the sensitivity of George VI Ice Shelf to changes in climatic conditions.

The bathymetry of the region further amplifies this vulnerability. Troughs in the continental shelf guide CDW into the cavity beneath the ice shelf (Fig. 1, Hyogo et al., 2024). Once inside the cavity, the CDW drives some of the highest basal melt rates observed in the Antarctic Peninsula (Davison et al., 2023).

3 Data and Methods

In the following subsections, we describe the data and methods used to i) generate high-resolution surface elevation and basal melt rates to analyze the temporal evolution of the channel (Sect. 3.1); ii) explore potential drivers behind the channel, utilizing both ice velocity observations (Sect. 3.2) and model simulations of ocean circulation and forcing (Sect. 3.3); iii) model temporal changes in basal melt patterns near the channel driven by variations in ocean forcing and ice shelf geometry (Sect. 3.4).

3.1 Surface elevations and basal melt rates

To derive high-resolution surface elevation and basal melt rates of the George VI Ice Shelf, we use BURGEE as presented in Zinck et al. (2023) and updated in Zinck et al. (2024a). In summary, BURGEE utilizes CryoSat-2 SARin Baseline-E Level 1B radar altimetry data to co-register the 2-meter REMA digital surface model strips (Howat et al., 2022), producing high-resolution surface elevation maps. From these maps, surface elevation changes are calculated in a Lagrangian framework, from which basal melt rates are derived using information about surface mass balance, firn, and ice flow.

For this study, we use REMA strips from version s2s041 (Howat et al., 2022) instead of the older s2s030 (REMA v1) used in Zinck et al. (2023, 2024a). The latter is the only version available on the Google Earth Engine but covers only the years from 2010 to 2017, whereas the newest version is updated yearly with new data. Since George VI is frequently cloud-covered, we included these newer strips to enhance coverage. All strips were bicubically interpolated onto a 50-meter grid from their original 2-meter resolution to reduce storage requirements, both locally and on Google Earth Engine.

Surface elevations were derived by co-registering the REMA strips to CryoSat-2 radar altimetry measurements, following the method outlined in Zinck et al. (2023) with updates from Zinck et al. (2024a). First, both datasets were adjusted for dynamic and static corrections – accounting for tides, mean dynamic topography, the inverse barometer effect, and geoid referencing. Then, tilt and bias in the REMA strips were corrected by fitting a plane through the REMA/CryoSat-2 elevation residuals. Basal melt rates were calculated similarly to Zinck et al. (2024a), with a minor adjustment in the Lagrangian displacement related to the feature tracking. In previous work (Zinck et al., 2024a), strips were referenced to a median elevation map covering the period 2015-07-01 to 2017-07-01. Here, for the George VI Ice Shelf, we extended this median elevation map period to 2018-07-01 for improved ice shelf coverage, resulting in better quality of the Lagrangian displacement. To derive the basal melt rate through the traditional mass conservation approach we used both information about firn air content from the IMAU-FDM v1.2A (Veldhuijsen et al., 2023) and surface velocities from MEaSURE ITS_LIVE (Gardner et al., 2022) to calculate the ice flux divergence as described in Zinck et al. (2023). For the surface mass balance, however, we used a new 2 km resolution

https://doi.org/10.5194/egusphere-2025-573
Preprint. Discussion started: 19 March 2025

downscaled version of the regional climate model RACMO (Noël et al., 2023). The final surface elevation and basal melt maps were produced on a 50-meter grid.

3.2 Ice velocities and divergences across the channel

To investigate ice speed and divergence across the new channel (Fig. 1), and track their temporal evolution as possible indicators of fracturing, we use monthly ice velocities from ENVEO (provided by the European Space Agency's Antarctic Ice Sheet Climate Change Initiative project). Based on Sentinel-1 (synthetic aperture radar) imagery, these velocities offer higher spatial and temporal resolution, along with greater coverage, compared to velocity products based on optical imagery feature tracking. We examine a ∼15 km transect crossing both the persistent channel system and the new channel (Fig. 1). Yearly ice speeds are calculated by taking the median of the monthly speeds, with measurements extracted every ∼250 meters along the transect.

To obtain the divergence along the transect, we first calculate the yearly median x- and y-components of the monthly velocity fields, then extract the values along the transect in the same manner as for ice speed. The divergence is computed by summing the velocity gradients in the x- and y-directions for the yearly velocity fields along the transect. To estimate the noise in the divergence data we calculate the root-mean-square error of the yearly divergences along a transect (Divergence comparison, Fig. 1) where rifting and thus changes in the divergence field are not expected to occur.

3.3 Ocean heat and circulation

To investigate changes in ocean heat content and circulation during the study period, we use output from the Amundsen-Bellingshausen Seas regional configuration of the Massachusetts Institute of Technology general circulation model (MITgcm), which has been validated against observational oceanographic data (Hyogo et al., 2024; Park et al., 2024). This model configuration, originally developed by Nakayama et al. (2018), features a horizontal grid spacing of 2–4 km and 70 vertical layers. The vertical resolution varies, with layer thicknesses ranging from 10 meters near the surface to 450 meters in the deepest regions (∼ -6000 m), and between 70–90 meters at depths of -500 to -1000 meters. The model uses constant ice shelf geometry and ocean bathymetry from BEDMAP-2 (Fretwell et al., 2013) and has a monthly temporal resolution. We use the model for two purposes; to analyze changes in i) ocean circulation and ii) ocean heat. First, to explore potential changes in ocean circulation near the channel which could explain its development, we obtain mean annual velocities by averaging the model's monthly velocities over the years 2010 and 2020, at two different depth levels: -325 m and -391 m. The first is just below the ice base in the thinner areas and the latter is at a depth below the ice base in most areas near the channel. Secondly, to investigate changes in ocean heat we examine monthly changes in temperature and salinity for all years between 2010 and 2020 to determine if shifts in ocean heat potential can explain the channel's development. Temperature and salinity profiles are extracted from three cross-sections: the northern and southern entrances to the ice shelf cavity, and near the channel (Fig. 1). Even though the new channel is located near the southern entrance, CDW entering through the northern entrance might contribute to the meltwater plume within the channel system, due to the sub-shelf circulation (Hyogo et al., 2024). Anomalies in temperature and salinity are calculated by subtracting the 2010 to 2020 time-averaged values at each depth level. Furthermore, we compute

https://doi.org/10.5194/egusphere-2025-573
Preprint. Discussion started: 19 March 2025

the depth-averaged monthly temperature and salinity for the water mass below -300 m, where CDW is found in the George VI cavity (Jenkins and Jacobs, 2008; Holland et al., 2010).

3.4 Modelling of basal melt rates

We use the two-dimensional basal melt model LADDIE (Lambert et al., 2023) to simulate basal melt rates with greater spatial detail (compared to the MITgcm output) for George VI Ice Shelf in two scenarios: i) from the beginning of the BURGEE period before July 2016 (BEFORE experiment), and ii) from the end of the BURGEE period after July 2016 (AFTER experiment). The goal is to investigate potential changes in plume direction and melt patterns near the channel, using two different ice shelf geometries and ocean forcings, resembling the two different time periods, while keeping other model parameters constant. Below, we describe how these ice shelf geometries and ocean forcings are derived, and how the model is tuned to match observed basal melt rates.

3.4.1 Ice shelf geometry

The ice shelf geometries for the BEFORE and AFTER scenarios are generated using a combination of BedMachineV3 (Morlighem et al., 2020; Morlighem, 2022) data and co-registered REMA strips (Sect. 3.1). BedMachineV3 provides the bathymetry, ice shelf mask, and the ratio between surface elevation and ice shelf thickness, which we use to transform REMA-derived surface elevations into ice thickness and draft. As LADDIE only considers areas where its mask is set to be ice shelf, we do not consider areas outside of the ice shelf in terms of the generation of the BEFORE and AFTER geometries.

We use BURGEE to create two separate high-resolution surface elevation maps of the ice shelf (see Fig. 2 for a visual representation of the workflow). This implies horizontally aligning REMA strips from different time periods, followed by a vertical alignment with respect to BedMachineV3. For the surface elevation for the BEFORE geometry, all strips up to 2016-07-01 are firstly displaced to their location as of 2013-01-01 using MEaSURES ITS_LIVE velocities (Gardner et al., 2022). Secondly, these strips are further displaced using feature tracking relative to the median elevation map between 2012-07-01 and 2015-07-01 to ensure alignment across strips. The displaced strips provide surface elevation estimates. To derive ice thickness, we use BedMachineV3's surface-elevation-to-thickness ratio. Since the surface elevation used in BedMachineV3 has not been subject to the exact same dynamic and static corrections as used here, the finally co-registered strips are co-registered to the BedMachineV3 surface, by fitting a plane through the residuals. The median of the resulting strips is taken and interpolated onto the 500 m BedMachineV3 grid, from which ice shelf thickness is obtained by using the BedMachineV3 surface elevation to thickness ratio. All negative ice shelf thicknesses and ice shelf thicknesses $>$ 2000 m are replaced by BedMachineV3 thicknesses, as well as all other remaining gaps. The same procedure is followed for the AFTER geometry, considering all strips from 2016-07-01 to 2022-12-31, displaced to 2023-01-01. The feature tracking displacement is performed using the median elevation map between 2018-07-01 and 2022-12-31. The surface elevation in BedMachineV3 is based on the REMA mosaic generated from the strips from 2010-2017, so to reduce inconsistencies in the grounding zone area, we mask out the grounding zone ($\sim$1.5 km) in the median (AFTER) surface elevation map and replace the surface elevation here with that from the BEFORE surface elevation map. The replacement is done with the BEFORE elevation map instead of BedMachineV3

https://doi.org/10.5194/egusphere-2025-573
Preprint. Discussion started: 19 March 2025

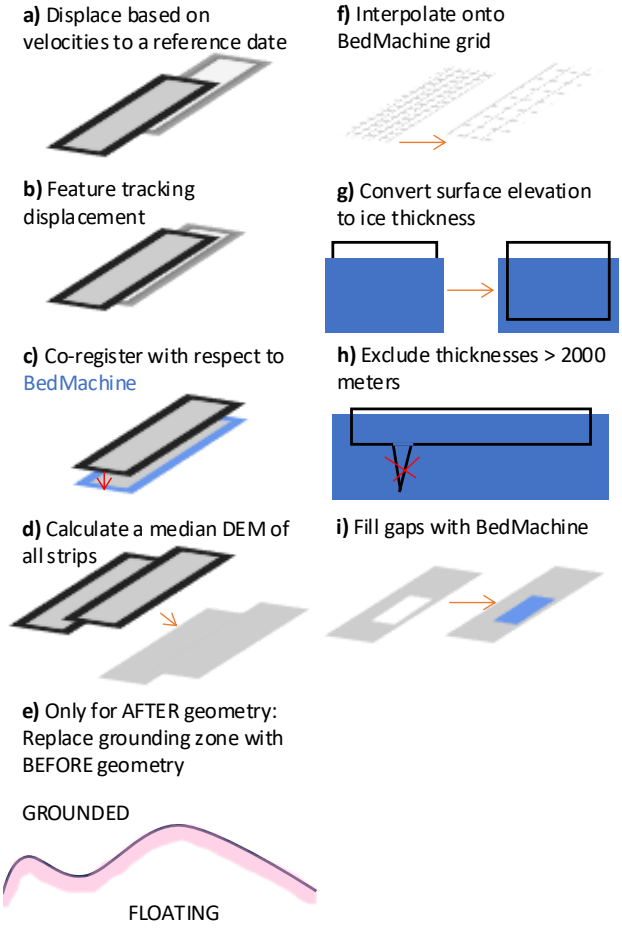

Figure 2. The workflow used to generate the BEFORE and AFTER geometries. The grounding line masking in **(e)** is only done for the AFTER geometry.

to allow for greater spatial details. Like, the BEFORE geometry, ice thickness outliers and all remaining gaps are filled with BedMachineV3 values.

3.4.2 Ocean forcing

We force LADDIE with a 1D temperature and salinity profile (Lambert et al., 2023) based on MITgcm results from 2010 and 2020 (Hyogo et al., 2024), for the BEFORE and AFTER experiment, respectively. We average the May-August MITgcm temperatures and salinities from the Northern and Southern profiles (Fig. 1) to obtain the average forcing for 2010 and 2020 (Fig. 3). We only consider Austral winter months (May-August) to reduce the noise level from the seasonality in the upper ocean layers. To avoid sudden changes in temperature and salinity present in the MITgcm outputs and to ensure a stable stratification, we describe both salinity and temperature as a tangent hyperbolic function. For the temperature, the tangent

https://doi.org/10.5194/egusphere-2025-573
Preprint. Discussion started: 19 March 2025

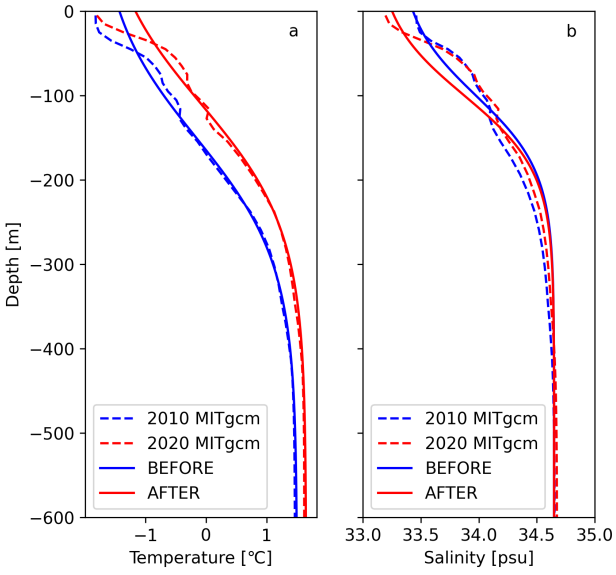

Figure 3. Average temperature **(a)** and salinity **(b)** profiles from winter months (May-August) of MITgcm in 2010 (dashed blue) and 2020 (dashed red), alongside with the tangent hyperbolic prescribed temperate **(a)** and salinity **(b)** used in LADDIE for the BEFORE run (solid blue) and AFTER run (solid red).

hyperbolic function is already built into LADDIE, where the surface temperature (T_0) is based on the surface salinity (S_0) following

$$T_0 = l_1 S_0 + l_2. \tag{1}$$

Here l_1 and l_2 are the freezing point salinity coefficient and the freezing point offset, respectively. The temperature (T) as a function of depth (z) is then given by

$$T(z) = T_1 + (T_0 - T_1)\frac{1 + \tanh\left(\frac{z - z_0}{z_1}\right)}{2}, \tag{2}$$

where T_1 is the temperature at depth, z_0 is the reference depth for the thermocline, and z_1 is the scaling factor of the thermocline, which determines the thermocline gradient. The salinity is in LADDIE, however, described by a quadratic function, which does not fit well with the MITgcm outputs, as they roughly follow the same profile as the temperature (Fig. 3). We, therefore, use a similar tangent hyperbolic function for the salinity (S) as for the temperature, following

$$S(z) = S_1 + (S_0 - S_1)\frac{1 + \tanh\left(\frac{z - z_{0,S}}{z_{1,S}}\right)}{2}. \tag{3}$$

Here, S_1 is the salinity at depth, $z_{0,S}$ is the halocline reference depth (as opposed to the thermocline for the temperature), and $z_{1,S}$ is the halocline scaling factor. Surface salinity, salinity at depth, and temperature at depth are all roughly based on the MITgcm profiles, whereas the thermocline/halocline depths and scaling factors are tuned to match the MITgcm profiles.

https://doi.org/10.5194/egusphere-2025-573
Preprint. Discussion started: 19 March 2025

Table 1. Forcing parameters used in the BEFORE and AFTER experiments.

Parameter	BEFORE	AFTER
Temperature at depth, T_1 [°C]	1.50	1.65
Thermocline depth, z_0 [m]	-150	-110
Thermocline scaling factor, z_1 [m]	150	150
Freezing point salinity coef., l_1 [°C/psu]	3.733e-5	3.733e-5
Freezing point offset, l_2 [°C]	8.32e-2	8.32e-2
Surface salinity, S_0 [psu]	33.30	33.10
Salinity at depth, S_1 [psu]	34.65	34.65
Halocline depth, $z_{0,S}$ [m]	-100	-100
Halocline scaling factor, $z_{1,S}$ [m]	90	90

For both temperature and salinity the tangent hyperbolic only starts to diverge from the MITgcm profiles at depths above ∼-100 m (Fig. 3), which is shallower than the ice shelf draft in most parts of the ice shelf with the exception of a few areas in the northern part of the ice shelf. All forcing parameters for the BEFORE and AFTER experiments are tabulated in Tab. 1.

3.4.3 Tuning

Ocean models approximate physical processes, which implies that they need to be tuned in order to match observations. LADDIE has two tuning parameters; the minimum meltwater layer thickness (D_{min}) and the drag coefficient ($C_{d,top}$) applied to the friction velocity in the basal melting formulation (Lambert et al., 2023). We use the latter as the main tuning parameter due to its direct influence on basal melt rates as tuning $C_{d,top}$ roughly corresponds to scaling the basal melting magnitude up and down. To calibrate the model, we iteratively adjust $C_{d,top}$ to approximate the maximum BURGEE melt rates observed near the channel of interest using the BEFORE geometry. Once determined, this value of $C_{d,top}$ remains fixed across the BEFORE and AFTER experiments, allowing us to focus on the effects of changing geometry and forcing. The full list of model parameters specific for our experiments is provided in Tab. 2.

4 Results

The basal melt rate trend from 2010 to 2022, shown in Fig. 1, reveals a general pattern consistent with previous studies (Davison et al., 2023): higher melt rates are observed in the southern region of the ice shelf compared to the north. Furthermore, as is typical for most ice shelves, the highest melt rates are concentrated near the grounding zone, with channels extending from these zones across mainly the southern part of the ice shelf. A closer examination of the newly identified channel highlights its position within a densely channelized area. This channel stands out with exceptionally high melt rates, reaching up to

https://doi.org/10.5194/egusphere-2025-573
Preprint. Discussion started: 19 March 2025

Table 2. LADDIE parameters used in both experiments.

Parameter	Value
Time step [s]	36
Horizontal resolution [m]	500
Equilibrium time [model days]	60
Top drag coefficient, $C_{d,top}$	$3.0{\cdot}10^{-4}$
Minimum thickness, D_{min} [m]	2
Ice temperature [°C]	-25
Tidal velocity [m/s]	0.01
Horizontal viscosity [m^2/s]	6
Horizontal diffusivity [m^2/s]	1

approximately 30 m/yr, which surpasses the melt rates in the surrounding channels. The channel appears to intersect existing channels, complicating the interpretation of the meltwater plume's pathway.

By examining the surface elevations over the study period, it becomes evident that the new channel has developed during this period; it began forming around 2015, reflected by a narrow surface depression in Fig. 4d. This depression deepens progressively throughout the study period by 23 m between 2013/14 and 2022/2023, with two further key observations emerging. First, as the depression associated with the channel becomes more pronounced (Fig. 4j, around 11 km), the deepest part of the older channel becomes shallower (Fig. 4j, around 8 km), while the flanks of the older channel are lowering (Fig. 4j, around 4-8 km and 9-10 km), thereby widening this pre-existing channel. These flanks are also associated with high melt rates ($\sim$ 15 m/yr, Fig. 1), as opposed to the deepest part of the channel ($\sim$ 0 m/yr, Fig. 1). The continuous lowering of the flanks suggests that the channel system is not in a steady state, with the closure of the deepest part possibly indicating channel re-routing, where the new channel may now serve as the primary basal melt pathway. Second, just downstream of the channel (Fig. 4j, around 12 km) a slight surface elevation bump appears from 2016/17 onward. This type of bump, known as flanking uplift, is typically associated with fractures on ice shelves (Walker and Gardner, 2019). These findings suggest that the channel could either be a fracture, a basal melt channel, or a combination of both (i.e., a fracture that serves as a melt plume pathway or a channel that has begun to fracture). Since both basal channels and fractures can weaken ice shelves (Alley et al., 2022, 2024), the presence of either on George VI, a relatively thin ice shelf with a relatively warm atmosphere, likely contributes to its weakening (Smith et al., 2007).

To further investigate fracturing as a possible driver behind such a fast developing channel we explore changes in ice flow across the channel. Ice shelf fracturing is typically linked to variations in ice speed and divergence caused by stretching. Our analysis of ice speed and divergence across the channel show speeds along the transect fluctuating substantially in both 2014/15 and 2015/16 (Fig. 5a and b) from $\sim$370 m/yr to almost $\sim$400 m/yr with an isolated peak in the ice speed at the channel location in 2015/16. That peak is associated with sudden changes in divergence from -0.02 m/yr (compression) just upstream of the

https://doi.org/10.5194/egusphere-2025-573
Preprint. Discussion started: 19 March 2025

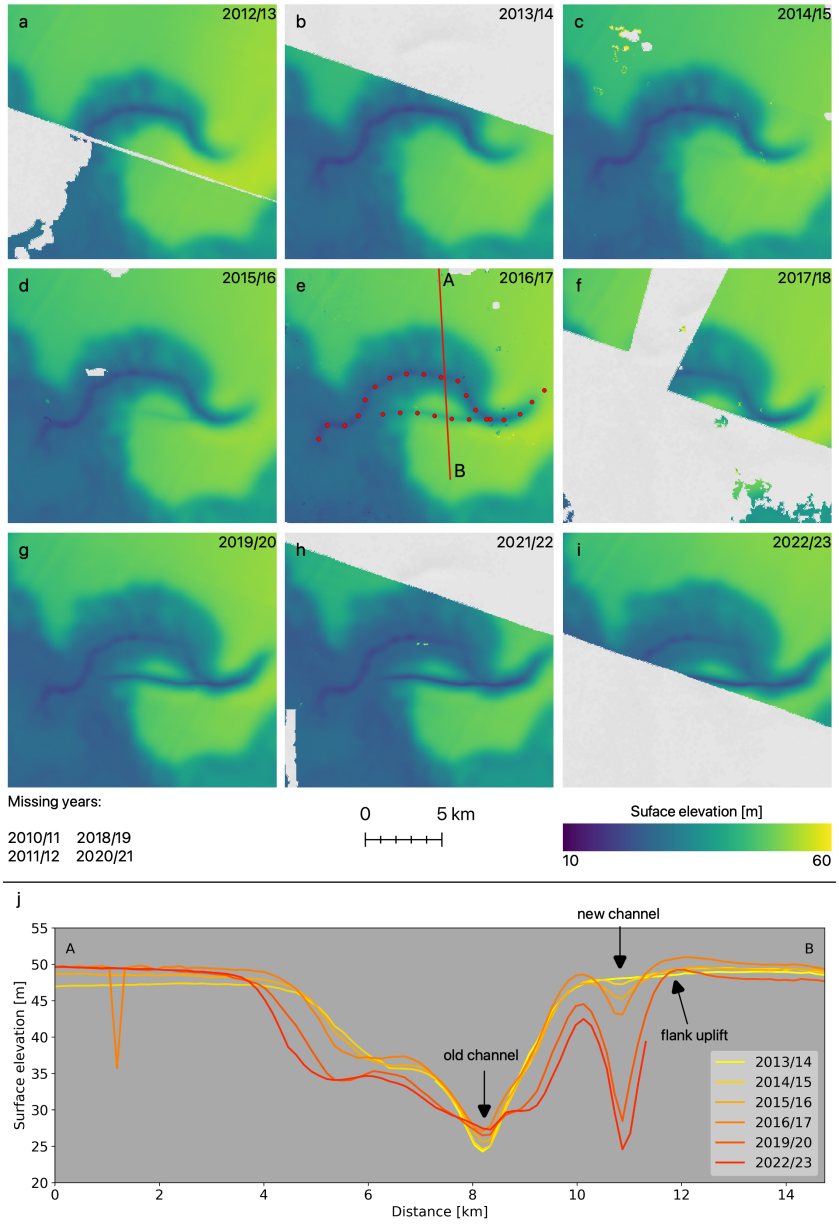

Figure 4. **(a-i)** surface elevations through time from 2012/13 in **(a)** to 2022/23 in **(i)**. In panel e the old/persistent and new channel are marked by red dots. The missing years indicated in the legend are years without REMA coverage in this area. **(j)** shows the surface elevations in a Lagrangian framework along the transect marked and lettered for direction in **(e)** which crosses both the persistent channel (surface depression deepest at around 8.2 km) and the new channel (around 11 km). The sudden dip around 1 km in one of the surface elevations is caused by a few contaminated pixels in that given REMA strip.

https://doi.org/10.5194/egusphere-2025-573
Preprint. Discussion started: 19 March 2025

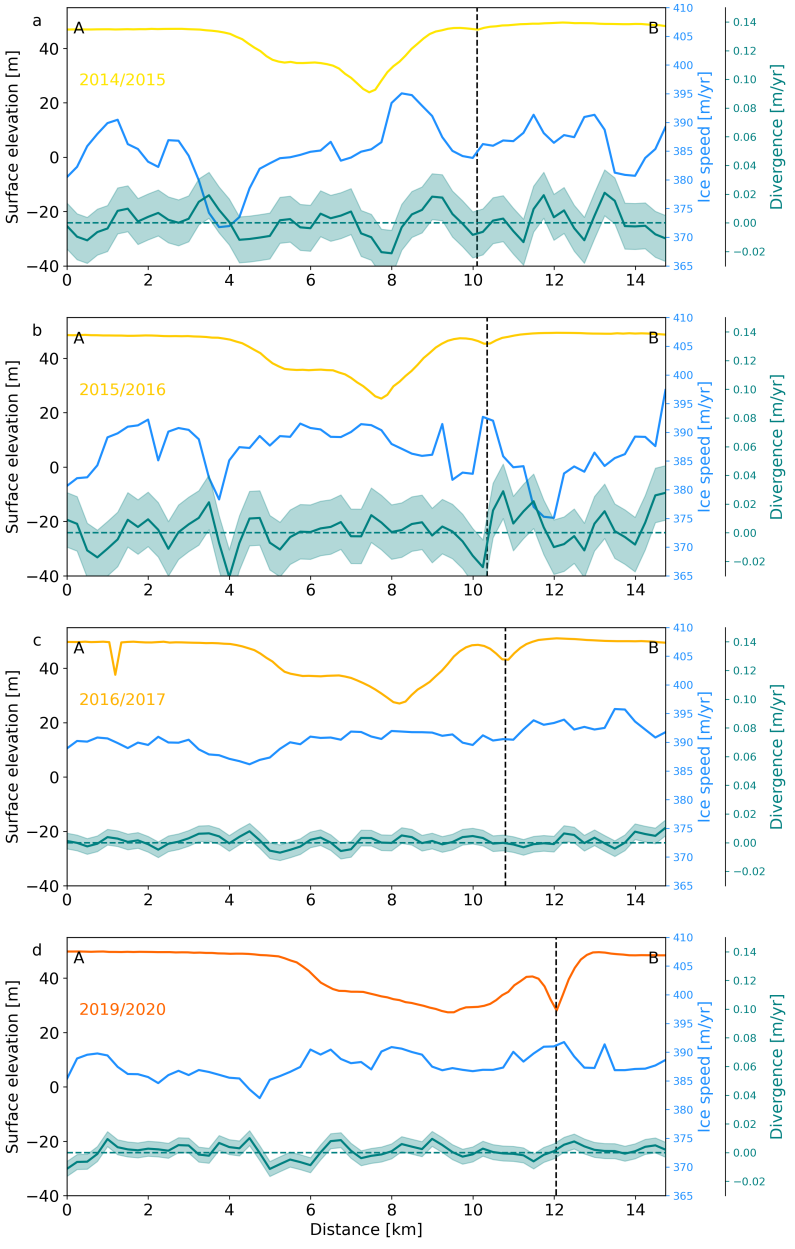

Figure 5. Surface elevation (same coloring as in Figure 4j), ice speed (blue) and divergence (green), all in a Eulerian framework, along the transect marked in Figure 4e. The dashed green line indicate zero divergence, to easier distinguish between stretching (positive values) and compression (negative values). The shaded green area indicates the noise in the signal as described in Sect. 3.2. The dashed black line marks the approximate location of the channel. **(a)** is year 2014/15, **(b)** is 2015/16, **(c)** is 2016/17, and **(d)** is 2019/20.

https://doi.org/10.5194/egusphere-2025-573
Preprint. Discussion started: 19 March 2025

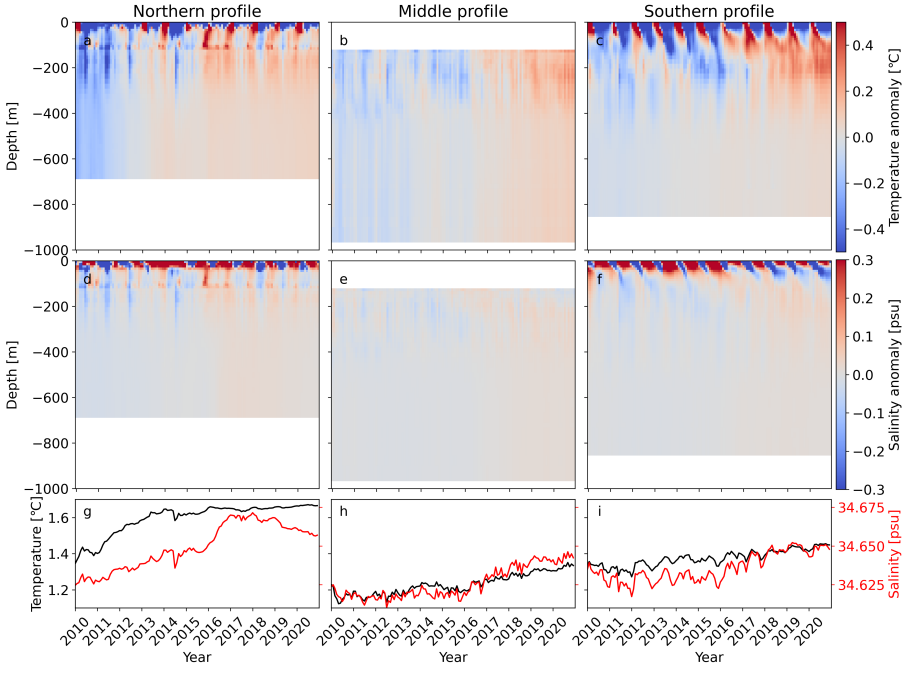

Figure 6. MITgcm ocean temperature (**a**-**c**) and salinity (**d**-**f**) anomalies of the Northern profile (**a** and **d**), Middle profile (**b** and **e**), and Southern profile (**c** and **f**) as marked in Figure 1. Panel **g**-**i** show the average temperature and salinity at all depths <-300 m through time of the Northern profile (**g**), Middle profile (**h**) and Southern profile (**i**).

channel to 0.03 m/yr (stretching) just downstream of the channel (10-11 km, Fig. 5b), which could indicate fracturing as a potential driver of the channel. These changes, however, are rather subtle in comparison to the noise level and to observations across wider fractures ($\sim$ 1-4 km) on e.g. Ross Ice Shelf, where divergences reaches 30-80 m/yr at their maximum (Walker and Gardner, 2019). The low magnitude of the changes could potentially be due to the coarse resolution of the velocity product (200 m) relative to the channel's width and depth. Finally, in the later years (2017 and 2020, Fig. 5c and d), both ice speeds and divergences are more stable, without any outstanding signals in the vicinity of the channel.

Focusing on changes in ocean heat as possible driver of channel changes, we investigate temporal changes in ocean temperature and salinity. Figure 6a-f illustrate temperature and salinity anomalies for the Northern, Middle, and Southern profiles (Fig. 1), revealing a regime shift from cold and fresh conditions to warmer and saltier conditions across all profiles. At the Northern profile, this shift begins around 2013, intensifying in 2015/16, after which sub-shelf temperatures remain above the temporal mean. Similar, albeit weaker, trends are observed in the Middle and Southern profiles. In the deeper ocean layers below -300 m, where CDW resides, both average temperature and salinity have increased over the study period across all three profiles (Fig. 6g-i). Notably, a jump in salinity is observed around 2016, with the most pronounced increase in the Northern profile (Fig. 6g), where the strongest temperature and salinity anomaly shifts also occur (Fig. 6a and d), although the average temperature at depth already starts increasing in 2011 (Fig. 6g). This shift in ocean regime aligns with the 2015 El Niño

https://doi.org/10.5194/egusphere-2025-573
Preprint. Discussion started: 19 March 2025

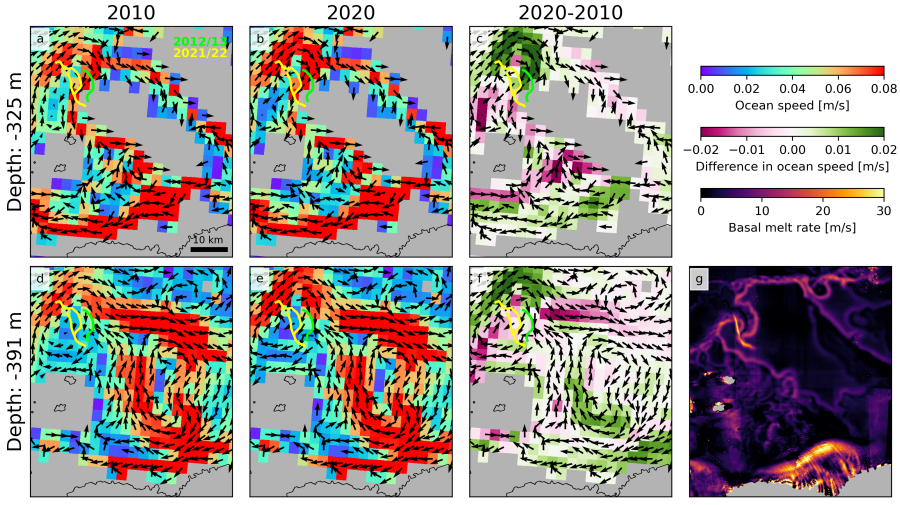

Figure 7. Yearly averaged ocean circulation in the vicinity of the channel in 2010 ((**a**) and (**d**)), 2020 ((**b**) and (**e**)), and the difference between the two ((**c**) and (**f**)) at two different depths (-325 m in (**a-c**) and -391 m in (**d-f**) which roughly corresponds to the layers right below the ice shelf base. The arrows in panel (**c**) and (**f**) correspond to the ocean circulation directions in 2020. The locations of the original and the new channel from 2012/13 and 2021/22 are marked in green and yellow, respectively. The BURGEE melt rates in (**g**) are shown for easier orientation.

Southern Oscillation (ENSO) event, with its effects already having been shown to reach George VI (Boxall et al., 2024). These changes in oceanic conditions, partially driven by ENSO, thus indicate more heat available for basal melting, likely intensifying and accelerating the meltwater plume, which in turn may cause higher melt rates and alterations in the plume pathway, influenced by the ice shelf's evolving geometry. Furthermore, in the Southern temperature anomaly profile, where several melt channels have their outflow (Fig. 1), the upper ocean layers have become fresher since 2016 (Fig. 6f), possibly indicating increased meltwater outflow.

In addition to changes in ocean temperature and salinity, MITgcm model outputs suggest alterations in ocean circulation near the channel (Fig. 7). Although there is a disparity in scale between the model grid size and the size of the channel, we can reasonably conclude that changes in ocean circulation likely occurred near the channel between 2010 and 2020, with higher current velocities near the channel. However, interpreting circulation changes in more detail and on a smaller scale, particularly in the immediate vicinity of the channel, remains challenging given the coarse model resolution.

The LADDIE model outputs from the BEFORE and AFTER experiments allow us to zoom in on the channel at a finer resolution, enabling us to explore how changes in ice shelf geometry and ocean forcing affect basal melt patterns. The modeled melt rate patterns (Fig. 8) align well with observations in areas outside the channel (Fig. 1). Figure 8f shows that LADDIE suggests the channel could serve as a pathway for the meltwater plume, potentially contributing to the high melt rates within the channel itself. Moreover, both BEFORE and AFTER melt patterns show enhanced melt along the sides of the channel, similar to BURGEE, which explains the widening of the old channel seen in Fig. 4j. Notably, the observed BURGEE melt

https://doi.org/10.5194/egusphere-2025-573
Preprint. Discussion started: 19 March 2025

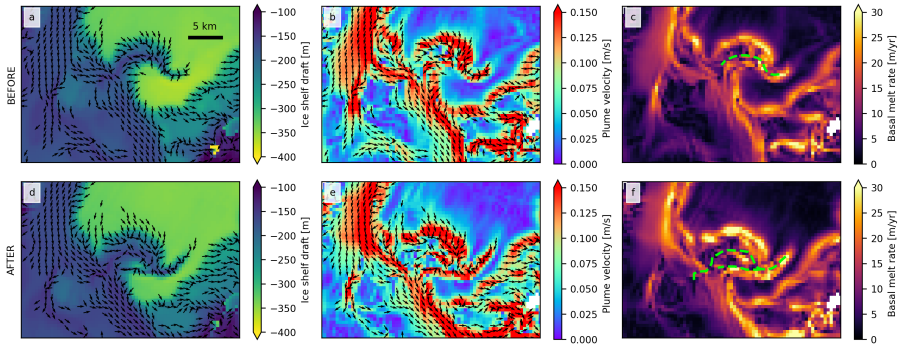

Figure 8. **(a-c)** Ice shelf draft, plume velocity, and basal melt rate in the BEFORE experiment. **(d-f)** Same as **(a-c)** but for the AFTER experiment. Arrows on the ice shelf draft ((**a**) and (**d**)) are the plume velocities. The dashed green line in **(c)** marks the location of the original channel in 2012/13 and the dashed green line **(f)** marks the location of the new channel in 2021/22.

pattern (Fig. 1) near the channel appears to combine elements from both the BEFORE and AFTER experiments, with channels following the "original" channel system as in the BEFORE scenario combined with high melt rates within the new channel as in the AFTER scenario. This strong agreement between observations and models suggests that the plume pathway may have shifted during the BURGEE observational period, now following a new route as indicated by the AFTER experiment.

5 Discussion

In this study, we uncovered a new channel within the channelized basal melting network of the George VI Ice Shelf, characterized by rapid changes in surface elevation, from 48 m in 2013/14 to 25 m in 2022/23. The onset of this channel coincides with both a shift towards a warmer ocean regime as well as subtle divergence changes across the channel, both aligning with the 2015 ENSO event (Boxall et al., 2024). ENSO has already been linked to an intensified inflow of CDW onto the continental shelf during El Niño years (Huguenin et al., 2024), supporting the MITgcm results of a warmer regime after 2015. The 2015 ENSO event has further been linked to the acceleration of glaciers feeding into the George VI Ice Shelf (Boxall et al., 2024). ENSO events have additionally been shown to enhance basal melting on ice shelves in the Amundsen Sea Sector (Paolo et al., 2018). While we cannot definitively conclude that ENSO caused the appearance of this channel, the timing is notable and the potential link to ENSO is important, as the projected increase in El Niño frequency suggest even further acceleration of ice shelf basal melting in Antarctica in the future (Cai et al., 2023).

The observed new channel could represent a basal melt channel, a fracture, or a combination of both and our investigations of the channel's origin point towards both the latter. The uplift in the surface near the depression, coupled with signs of stretching in the divergence field downstream of the channel in 2015/16, suggests fracturing. However, these signals are subtle, leaving us unable to confirm or dismiss the possibility of fracturing with certainty. At the same time, changes in ocean temperature, salinity, and circulation point to evolving and strengthening basal melt conditions that could encourage channel re-routing.

https://doi.org/10.5194/egusphere-2025-573
Preprint. Discussion started: 19 March 2025

Our LADDIE modelling results further support this possibility, indicating that even if the channel originated as a fracture, the meltwater plume may now be using it as a new pathway, which could further deepen the fracture, provided the initial fracture has a basal component.

To assess the potential impact of the new channel on the weakening of George VI Ice Shelf, we can draw parallels to other ice shelves where interactions between basal melt channels and fractures have led to structural instability. A notable example is Pine Island Ice Shelf, where a channel first observed in the 1970s progressively thinned and extended over time (Alley et al., 2022, 2024). This channel triggered both transverse fractures and fractures along the channel's length, eventually leading to calving and retreat along the channel from approximately 2018 to 2022 (Alley et al., 2022, 2024). The new channel on George VI Ice Shelf is located just about 30 km from the southern edge, raising concerns that continued melting, thinning, and weakening in this region could drive significant structural changes. These changes may include enhanced fracturing, calving, and ultimately, retreat of the ice shelf in this highly channelized area. Given projections of increased ocean heat availability in the future (Naughten et al., 2023), basal melting is expected to intensify, further amplifying the vulnerability of this portion of George VI Ice Shelf.

To definitively determine whether the channel is a fracture, a basal melt channel, or a combination of the two, in-situ field measurements, including basal melt rates, ice deformation monitoring, and radar surveys of ice thickness, are necessary. Regardless of its specific nature, this channel offers a direct observation of weakening in a highly channelized, vulnerable portion of the ice shelf. These results underscore how quickly ice shelf channels - important for ice shelf integrity - can occur and how easily small-scale changes might go unnoticed. Closely observing the continued evolution of the ice shelf and its integrity will be crucial in understanding these weakening processes. Such knowledge could also be valuable for other heavily channelized ice shelves, like Pine Island and Totten, which both have a higher projected potential sea level rise contribution.

6 Conclusions

Our study highlights the rapid emergence of a significant channel on the George VI Ice Shelf, marked by a 23 m surface lowering over just nine years. The appearance of the channel aligns with both changes in ocean forcing, most notably increased ocean temperatures and salinity, and subtle changes in ice divergence, both of which coincide with the timing of a major ENSO event. While the exact link between ENSO and the development of this channel remains speculative, the temporal correlation suggests that large-scale climate patterns may have a role in amplifying basal melting and possibly in re-routing meltwater pathways on Antarctic ice shelves.

The presence of such a fast-evolving channel on an already thin and vulnerable ice shelf like George VI likely has destabilizing effects, accelerating its weakening through both basal melting and fracturing. The behavior of this channel on George VI may offer valuable insights into how sudden changes in ocean forcing could trigger similar destabilizing processes elsewhere.

Moving forward, continuous monitoring of this channel and its evolving impact on George VI is crucial. The lessons learned from tracking its development may provide critical information on the future behavior of other highly channelized ice shelves

https://doi.org/10.5194/egusphere-2025-573
Preprint. Discussion started: 19 March 2025

undergoing changes in ocean conditions. Understanding these processes is essential for better projecting potential ice shelf retreat and the associated contributions to global sea-level rise.

Code and data availability. The BURGEE code is publicly available at https://github.com/aszinck/BURGEE (Zinck, 2023), likewise is LADDIE (https://github.com/erwinlambert/laddie). The derived melt rates as well as surface elevations are also publicly available (Zinck et al., 2024b). The REMA strips are available from the Polar Geosptaital Center (https://www.pgc.umn.edu/data/rema/) and CryoSat-2 data is available from the European Space Agency (https://earth.esa.int/eogateway/documents/20142/37627/CryoSat-Baseline-D-Product-Handbook.pdf). BedMachine V3 is available from NASA National Snow and Ice Data Center (https://nsidc.org/data/NSIDC-0756/versions/3) and MEaSUREs ITS_LIVE velocities are avialable from https://doi.org/10.5067/6II6VW8LLWJ7 and https://nsidc.org/data/NSIDC-0756/versions/3. The ENVEO monthly velocities provided by the European Space Agency's Antarctic Ice Sheet Climate Change Initiative project are available from https://cryoportal.enveo.at/data/. The regional MITgcm model output is available from https://ecco.jpl.nasa.gov/drive/files/ECCO2/LLC1080_REG_AMS/Hyogo_et_al_2022 (Hyogo et al., 2024).

Author contributions. The study was designed by ASPZ, BW, and SL and carried out by ASPZ. FJ made significant contributions in setting up the LADDIE experiments and interpreting the results therefrom. ASPZ wrote the paper with input from all authors.

Competing interests. BW and SL are members of the editorial board of The Cryosphere. The authors declare no further competing interests.

Acknowledgements. This study is part of the HiRISE project funded by the Dutch Research Council (NWO, no. OCENW.GROOT.2019.091). The authors would like to thank Shuntaro Hyogo for providing guidance on how to read the MITgcm data and Yoshihiro Nakayama for providing guidance on how interpret the MITgcm data.

https://doi.org/10.5194/egusphere-2025-573
Preprint. Discussion started: 19 March 2025

References

Alley, K. E., Scambos, T. A., Siegfried, M. R., and Fricker, H. A.: Impacts of warm water on Antarctic ice shelf stability through basal channel formation, Nature Geoscience, 9, 290–293, https://doi.org/10.1038/ngeo2675, 2016.

Alley, K. E., Scambos, T. A., and Alley, R. B.: The role of channelized basal melt in ice-shelf stability: recent progress and future priorities, Annals of Glaciology, 63, 18–22, https://doi.org/10.1017/aog.2023.5, 2022.

Alley, K. E., Alley, R. B., Crawford, A. D., Ochwat, N., Wild, C. T., Marson, J., Snow, T., Muto, A., Pettit, E. C., Child, S. F., Truffer, M., Collao-Barrios, G., and Scambos, T. A.: Evolution of sub-ice-shelf channels reveals changes in ocean-driven melt in West Antarctica, Journal of Glaciology, pp. 1–15, https://doi.org/10.1017/jog.2024.20, 2024.

Bamber, J. L., Oppenheimer, M., Kopp, R. E., Aspinall, W. P., and Cooke, R. M.: Ice Sheet and Climate Processes Driving the Uncertainty in Projections of Future Sea Level Rise: Findings From a Structured Expert Judgement Approach, Earth's Future, 10, 1–13, https://doi.org/10.1029/2022EF002772, 2022.

Boxall, K., Christie, F. D., Willis, I. C., Wuite, J., Nagler, T., and Scheiblauer, S.: Drivers of Seasonal Land-Ice-Flow Variability in the Antarctic Peninsula, Journal of Geophysical Research: Earth Surface, 129, https://doi.org/10.1029/2023JF007378, 2024.

Cai, W., Jia, F., Li, S., Purich, A., Wang, G., Wu, L., Gan, B., Santoso, A., Geng, T., Ng, B., Yang, Y., Ferreira, D., Meehl, G. A., and McPhaden, M. J.: Antarctic shelf ocean warming and sea ice melt affected by projected El Niño changes, Nature Climate Change, 13, 235–239, https://doi.org/10.1038/s41558-023-01610-x, 2023.

Chartrand, A. M. and Howat, I. M.: Basal Channel Evolution on the Getz Ice Shelf, West Antarctica, Journal of Geophysical Research: Earth Surface, 125, https://doi.org/10.1029/2019JF005293, 2020.

Davison, B. J., Hogg, A. E., Gourmelen, N., Jakob, L., Wuite, J., Nagler, T., Greene, C. A., Andreasen, J., and Engdahl, M. E.: Annual mass budget of Antarctic ice shelves from 1997 to 2021, Science Advances, 9, https://doi.org/10.1126/sciadv.adi0186, 2023.

de Roda Husman, S., Lhermitte, S., Bolibar, J., Izeboud, M., Hu, Z., Shukla, S., van der Meer, M., Long, D., and Wouters, B.: A high-resolution record of surface melt on Antarctic ice shelves using multi-source remote sensing data and deep learning, Remote Sensing of Environment, 301, 113 950, https://doi.org/10.1016/j.rse.2023.113950, 2024.

Doemgaard, M., Millan, R., Andersen, J., Scheuchl, B., Rignot, E., Izeboud, M., and Bjørk, A.: Half a century of extensive acceleration and grounding line retreat following the ocean driven collapse of Wordie Ice Shelf, https://doi.org/10.21203/rs.3.rs-4778150/v1, 2024.

Dow, C. F., Lee, W. S., Greenbaum, J. S., Greene, C. A., Blankenship, D. D., Poinar, K., Forrest, A. L., Young, D. A., and Zappa, C. J.: Basal channels drive active surface hydrology and transverse ice shelf fracture, Science Advances, 4, https://doi.org/10.1126/sciadv.aao7212, 2018.

Drews, R., Schannwell, C., Ehlers, T. A., Gladstone, R., Pattyn, F., and Matsuoka, K.: Atmospheric and Oceanographic Signatures in the Ice Shelf Channel Morphology of Roi Baudouin Ice Shelf, East Antarctica, Inferred From Radar Data, Journal of Geophysical Research: Earth Surface, 125, https://doi.org/10.1029/2020JF005587, 2020.

Dutrieux, P., Vaughan, D. G., Corr, H. F., Jenkins, A., Holland, P. R., Joughin, I., and Fleming, A. H.: Pine Island glacier ice shelf melt distributed at kilometre scales, Cryosphere, 7, 1543–1555, https://doi.org/10.5194/tc-7-1543-2013, 2013.

Dutrieux, P., Stewart, C., Jenkins, A., Nicholls, K. W., Corr, H. F. J., Rignot, E., and Steffen, K.: Basal terraces on melting ice shelves, Geophysical Research Letters, 41, 5506–5513, https://doi.org/10.1002/2014GL060618, 2014.

Fretwell, P., Pritchard, H. D., Vaughan, D. G., Bamber, J. L., Barrand, N. E., Bell, R., Bianchi, C., Bingham, R. G., Blankenship, D. D., Casassa, G., Catania, G., Callens, D., Conway, H., Cook, A. J., Corr, H. F. J., Damaske, D., Damm, V., Ferraccioli, F., Forsberg, R., Fujita,

https://doi.org/10.5194/egusphere-2025-573
Preprint. Discussion started: 19 March 2025

S., Gim, Y., Gogineni, P., Griggs, J. A., Hindmarsh, R. C. A., Holmlund, P., Holt, J. W., Jacobel, R. W., Jenkins, A., Jokat, W., Jordan, T., King, E. C., Kohler, J., Krabill, W., Riger-Kusk, M., Langley, K. A., Leitchenkov, G., Leuschen, C., Luyendyk, B. P., Matsuoka, K., Mouginot, J., Nitsche, F. O., Nogi, Y., Nost, O. A., Popov, S. V., Rignot, E., Rippin, D. M., Rivera, A., Roberts, J., Ross, N., Siegert, M. J., Smith, A. M., Steinhage, D., Studinger, M., Sun, B., Tinto, B. K., Welch, B. C., Wilson, D., Young, D. A., Xiangbin, C., and Zirizzotti, A.: Bedmap2: improved ice bed, surface and thickness datasets for Antarctica, The Cryosphere, 7, 375–393, https://doi.org/10.5194/tc-7-375-2013, 2013.

Fürst, J. J., Durand, G., Gillet-Chaulet, F., Tavard, L., Rankl, M., Braun, M., and Gagliardini, O.: The safety band of Antarctic ice shelves, Nature Climate Change, 6, 479–482, https://doi.org/10.1038/nclimate2912, 2016.

Gardner, A., Fahnestock, M., and Scambos., T.: MEaSUREs ITS_LIVE Regional Glacier and Ice Sheet Surface Velocities, Version 1, NASA National Snow and Ice Data Center Distributed Active Archive Center, https://doi.org/10.5067/6II6VW8LLWJ7, 2022.

Holland, P. R., Jenkins, A., and Holland, D. M.: Ice and ocean processes in the Bellingshausen Sea, Antarctica, Journal of Geophysical Research: Oceans, 115, 1–16, https://doi.org/10.1029/2008JC005219, 2010.

Howat, I., Porter, C., Noh, M.-J., Husby, E., Khuvis, S., Danish, E., Tomko, K., Gardiner, J., Negrete, A., Yadav, B., Klassen, J., Kelleher, C., Cloutier, M., Bakker, J., Enos, J., Arnold, G., Bauer, G., and Morin, P.: The Reference Elevation Model of Antarctica - Strips, Version 4.1, https://doi.org/10.7910/DVN/X7NDNY, 2022.

Huguenin, M. F., Holmes, R. M., Spence, P., and England, M. H.: Subsurface Warming of the West Antarctic Continental Shelf Linked to El Niño-Southern Oscillation, Geophysical Research Letters, 51, https://doi.org/10.1029/2023GL104518, 2024.

Hyogo, S., Nakayama, Y., and Mensah, V.: Modeling Ocean Circulation and Ice Shelf Melt in the Bellingshausen Sea, Journal of Geophysical Research: Oceans, 129, 1–19, https://doi.org/10.1029/2022JC019275, 2024.

IPCC: Climate Change 2021 – The Physical Science Basis, Cambridge University Press, https://doi.org/10.1017/9781009157896, 2023.

Jenkins, A. and Jacobs, S.: Circulation and melting beneath George VI Ice Shelf, Antarctica, Journal of Geophysical Research: Oceans, 113, 1–18, https://doi.org/10.1029/2007JC004449, 2008.

Lambert, E., Jüling, A., van de Wal, R. S. W., and Holland, P. R.: Modelling Antarctic ice shelf basal melt patterns using the one-layer Antarctic model for dynamical downscaling of ice–ocean exchanges (LADDIE v1.0), The Cryosphere, 17, 3203–3228, https://doi.org/10.5194/tc-17-3203-2023, 2023.

Morlighem, M.: MEaSUREs BedMachine Antarctica, Version 3 [Data Set]. Boulder, Colorado USA. NASA National Snow and Ice Data Center Distributed Active Archive Center., https://doi.org/https://doi.org/10.5067/FPSU0V1MWUB6, 2022.

Morlighem, M., Rignot, E., Binder, T., Blankenship, D., Drews, R., Eagles, G., Eisen, O., Ferraccioli, F., Forsberg, R., Fretwell, P., Goel, V., Greenbaum, J. S., Gudmundsson, H., Guo, J., Helm, V., Hofstede, C., Howat, I., Humbert, A., Jokat, W., Karlsson, N. B., Lee, W. S., Matsuoka, K., Millan, R., Mouginot, J., Paden, J., Pattyn, F., Roberts, J., Rosier, S., Ruppel, A., Seroussi, H., Smith, E. C., Steinhage, D., Sun, B., Broeke, M. R. v. d., Ommen, T. D. v., Wessem, M. v., and Young, D. A.: Deep glacial troughs and stabilizing ridges unveiled beneath the margins of the Antarctic ice sheet, Nature Geoscience, 13, 132–137, https://doi.org/10.1038/s41561-019-0510-8, 2020.

Nakayama, Y., Menemenlis, D., Zhang, H., Schodlok, M., and Rignot, E.: Origin of Circumpolar Deep Water intruding onto the Amundsen and Bellingshausen Sea continental shelves, Nature Communications, 9, 1–9, https://doi.org/10.1038/s41467-018-05813-1, 2018.

Naughten, K. A., Holland, P. R., and De Rydt, J.: Unavoidable future increase in West Antarctic ice-shelf melting over the twenty-first century, Nature Climate Change, 13, 1222–1228, https://doi.org/10.1038/s41558-023-01818-x, 2023.

Noël, B., van Wessem, J. M., Wouters, B., Trusel, L., Lhermitte, S., and van den Broeke, M. R.: Higher Antarctic ice sheet accumulation and surface melt rates revealed at 2 km resolution, Nature Communications, 14, 7949, https://doi.org/10.1038/s41467-023-43584-6, 2023.

https://doi.org/10.5194/egusphere-2025-573
Preprint. Discussion started: 19 March 2025

Paolo, F. S., Padman, L., Fricker, H. A., Adusumilli, S., Howard, S., and Siegfried, M. R.: Response of Pacific-sector Antarctic ice shelves to the El Niño/Southern Oscillation, Nature Geoscience, 11, 121–126, https://doi.org/10.1038/s41561-017-0033-0, 2018.

Park, T., Nakayama, Y., and Nam, S.: Amundsen Sea circulation controls bottom upwelling and Antarctic Pine Island and Thwaites ice shelf melting, Nature Communications, 15, 2946, https://doi.org/10.1038/s41467-024-47084-z, 2024.

Pattyn, F. and Morlighem, M.: The uncertain future of the Antarctic Ice Sheet, Science, 367, 1331–1335, https://doi.org/10.1126/science.aaz5487, 2020.

Pritchard, H. D., Ligtenberg, S. R. M., Fricker, H. A., Vaughan, D. G., van den Broeke, M. R., and Padman, L.: Antarctic ice-sheet loss driven by basal melting of ice shelves, Nature, 484, 502–505, https://doi.org/10.1038/nature10968, 2012.

Rignot, E., Jacobs, S., Mouginot, J., and Scheuchl, B.: Ice-shelf melting around antarctica, Science, 341, 266–270, https://doi.org/10.1126/science.1235798, 2013.

Silvano, A., Rintoul, S., and Herraiz-Borreguero, L.: Ocean-Ice Shelf Interaction in East Antarctica, Oceanography, 29, 130–143, https://doi.org/10.5670/oceanog.2016.105, 2016.

Smith, J. A., Bentley, M. J., Hodgson, D. A., and Cook, A. J.: George VI Ice Shelf: past history, present behaviour and potential mechanisms for future collapse, Antarctic Science, 19, 131–142, https://doi.org/10.1017/S0954102007000193, 2007.

van de Wal, R. S. W., Nicholls, R. J., Behar, D., McInnes, K., Stammer, D., Lowe, J. A., Church, J. A., DeConto, R., Fettweis, X., Goelzer, H., Haasnoot, M., Haigh, I. D., Hinkel, J., Horton, B. P., James, T. S., Jenkins, A., LeCozannet, G., Levermann, A., Lipscomb, W. H., Marzeion, B., Pattyn, F., Payne, A. J., Pfeffer, W. T., Price, S. F., Seroussi, H., Sun, S., Veatch, W., and White, K.: A High-End Estimate of Sea Level Rise for Practitioners, Earth's Future, 10, 1–24, https://doi.org/10.1029/2022EF002751, 2022.

van Wessem, J. M., van den Broeke, M. R., Wouters, B., and Lhermitte, S.: Variable temperature thresholds of melt pond formation on Antarctic ice shelves, Nature Climate Change, 13, 161–166, https://doi.org/10.1038/s41558-022-01577-1, 2023.

Vaughan, D. G., Corr, H. F. J., Bindschadler, R. A., Dutrieux, P., Gudmundsson, G. H., Jenkins, A., Newman, T., Vornberger, P., and Wingham, D. J.: Subglacial melt channels and fracture in the floating part of Pine Island Glacier, Antarctica, Journal of Geophysical Research: Earth Surface, 117, 1–10, https://doi.org/10.1029/2012JF002360, 2012.

Veldhuijsen, S. B. M., van de Berg, W. J., Brils, M., Kuipers Munneke, P., and van den Broeke, M. R.: Characteristics of the 1979–2020 Antarctic firn layer simulated with IMAU-FDM v1.2A, The Cryosphere, 17, 1675–1696, https://doi.org/10.5194/tc-17-1675-2023, 2023.

Walker, C. and Gardner, A.: Evolution of ice shelf rifts: Implications for formation mechanics and morphological controls, Earth and Planetary Science Letters, 526, 115 764, https://doi.org/10.1016/j.epsl.2019.115764, 2019.

Zinck, A.-S.: BURGEE, GitHub [code], https://github.com/aszinck/BURGEE, 2023.

Zinck, A.-S., Lhermitte, S., Wearing, M., and Wouters, B.: Exposure to Underestimated Channelized Melt in Antarctic Ice Shelves, Nature Climate Change [in review], NCLIM-24071992, pp. 0–26, https://doi.org/10.21203/rs.3.rs-4806463/v1, 2024a.

Zinck, A.-S. P., Wouters, B., Lambert, E., and Lhermitte, S.: Unveiling spatial variability within the Dotson Melt Channel through high-resolution basal melt rates from the Reference Elevation Model of Antarctica, The Cryosphere, 17, 3785–3801, https://doi.org/10.5194/tc-17-3785-2023, 2023.

Zinck, A.-S. P., Wouters, B., Jesse, F., and Lhermitte, S.: Dataset belonging to the article: Ocean-Induced Weakening of George VI Ice Shelf, https://doi.org/10.4121/dbf9ade9-9f85-49f4-89ba-3d8d8310c9e4.v1, 2024b.